Two-leg-ladder Bose-Hubbard models with staggered fluxes

Rashi Sachdeva,[1,][*] Friederike Metz,[1] Manpreet Singh,[2] Tapan Mishra,[2] and Thomas Busch[1]

[1]*Quantum Systems Unit, Okinawa Institute of Science and Technology Graduate University, Okinawa 904-0495, Japan*
[2]*Department of Physics, Indian Institute of Technology, Guwahati-781039, Assam, India*

We investigate the ground-state properties of ultracold atoms trapped in a two-leg ladder potential in the presence of an artificial magnetic field in a staggered configuration. We focus on the strongly interacting regime and use the Landau theory of phase transitions and a mean field Gutzwiller variational method to identify the stable superfluid phases and their boundaries with the Mott-insulator regime as a function of magnetic flux. In addition, we calculate the local and chiral currents of these superfluid phases, which show a staggered vortex-antivortex configuration. The analytical results are confirmed by numerical simulations using a cluster mean-field-theory approach.

I. INTRODUCTION

Ultracold bosonic atoms in optical lattices offer a unique platform to study models for periodic many-body physics in a clean and highly controllable setting. A wide range of flexible geometries to trap neutral atoms can be created by overlapping and interfering laser beams and interactions can be controlled via external magnetic fields or by choosing different atomic species. While the field was initially enthused by the prediction and realization of the paradigmatic superfluid to Mott-insulator transition in square lattices [1,2], many different situations have been investigated since then [3,4].

Recent progress in creating artificial gauge fields for ultracold atoms in discrete [5] as well as continuum systems [6] has opened up many avenues for the study of quantum phase transitions in the presence of magnetic fields. These fields are called artificial, as due to the charge neutrality of the atoms no Lorentz force exists and therefore real magnetic fields do not directly affect the center-of-mass variable.

The simplest way to mimic the effects of magnetic fields on charged systems in neutral atoms is by rotation [7], which probes superfluidity in the same way magnetic fields probe superconductivity. Furthermore, very high synthetic magnetic fields have been shown to be realizable using atoms in optical lattices, where the atomic motion and the internal degrees of freedom can be coupled by laser-assisted tunneling [8]. This has led to the successful implementation of uniform as well as staggered flux distributions in the strong field regime [8,9] and has enabled the realization of two-dimensional (2D) topological states with finite Chern numbers [10,11].

Theoretically, the presence of artificial magnetic fields can be included into the Bose-Hubbard model by using complex tunnel couplings [12]. The main effect of these can be observed even in the absence of interactions and the single-particle spectrum for bosons in a periodic potential in the presence of a strong magnetic field forms a self-similar structure known as the Hofstadter butterfly [13]. As the effective magnetic fields created in optical lattices can be much larger than what is possible in solid-state systems, these techniques bring the study of a wide range of Hamiltonians into reach that are inaccessible in condensed-matter physics.

Besides the realization of magnetic fields in extended 2D lattice systems, the effects of artificial magnetic fields were also studied in bosonic ladder geometries, where chiral currents and vortex and Meissner phases were predicted and observed [14–24,26]. While ladder systems can be seen as the smallest possible lattice structure, they possess additional and unique properties, for example, due to the absence of the requirement that the magnetic fields have to have rational values [17–20]. Furthermore, even though the above-mentioned Meissner and vortex phases can already be observed for non-interacting systems, interacting bosonic ladder systems with uniform flux also support various spontaneously symmetry-broken phases and chiral Mott insulator states [25].

Bosonic systems in the presence of uniform fluxes in quasi-one-dimensional (quasi-1D) ladder geometries and two-dimensional geometries have been studied in detail [14–24,26] both theoretically and experimentally. However, the existing work on bosons in quasi-one dimension subjected to staggered artificial magnetic fluxes is much less extensive. In particular, only recently studies by Dhar *et al.* [25] have revealed the connection between spontaneously broken symmetry phases and chiral Mott insulator phases in such systems at the fully frustrated points when the magnetic flux takes the values $\alpha = \pm\pi$. The technical difficulty to experimentally engineer magnetic fields alternating on the spatial scale of optical lattices has now been overcome [8,21–23], which fully justifies the study of this realisable model for the full range of staggered magnetic flux strength for the quasi-1D system. Similar to the case of uniform fluxes, staggered fluxes [27–30] can drive quantum phase transitions in the two-leg Bose Hubbard ladder systems and can enlarge the range of physical effects that can be investigated. Here we study the example of a single-component BEC trapped in such a geometry in the presence of a periodically flipped artificial
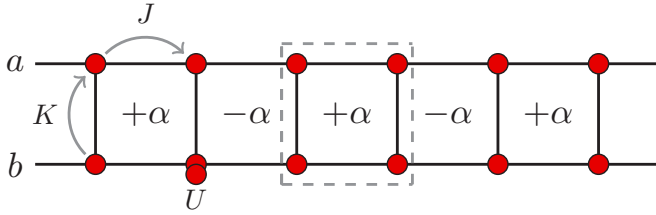
[*]rashi.sachdeva@oist.jp

FIG. 1. Schematic of the two-leg ladder Bose Hubbard model with staggered flux α in neighboring plaquettes. The dashed box indicates the single unit cell used for the analytic and the cluster mean field calculations. The red dots represent the bosonic atoms on lattice sites.

magnetic field. We find that the presence of the staggered flux gives rise to superfluid phases with staggered vortex-antivortex configurations, which are distinct from the usual superfluid phases obtained in the Bose-Hubbard model [1].

The paper is organized as follows. In Sec. II, we introduce the Bose-Hubbard model (BHM) with a two-leg ladder geometry in the presence of an artificial magnetic field with a staggered configuration. In Sec. III, we review the properties of its single-particle spectrum, and in Sec. IV, we present calculations in the strong coupling regime to determine the complete phase diagram. We also show the presence of flux-dependent superfluid phases using Landau theory. In Sec. V, we present our analytical calculations to determine the phase boundaries using the variational Gutzwiller approach, and in Sec. VI, these are complemented by the numerical calculations performed using the cluster mean field theory approach. Finally, in Sec. VII, we present a summary and outlook of the work.

II. MODEL

The Hamiltonian describing bosons in a two-leg ladder geometry in the presence of a staggered magnetic flux of magnitude α can be written as

$$
\begin{aligned}
H = & -J \sum_j \left[e^{(-1)^j \frac{i\alpha}{2}} a_j^\dagger a_{j+1} + e^{(-1)^{j+1} \frac{i\alpha}{2}} b_j^\dagger b_{j+1} + \text{H.c.} \right] \\
& - K \sum_j (a_j^\dagger b_j + \text{H.c.}) + \frac{U}{2} \sum_{j,p} n_j^p (n_j^p - 1) \\
& - \mu \sum_{j,p} n_j^p,
\end{aligned}
\tag{1}
$$

where the $p_j(p_j^\dagger)$ are the bosonic annihilation (creation) operators at site j of leg $p\ (=a, b)$, n_j^p is the number operator at site j of leg p, α is the absolute value of the magnetic flux, and μ is the chemical potential. The intra- and interleg hopping amplitudes are described by J and K respectively, and the on-site interaction energy between two atoms is given by U (see Fig. 1). The ratios J/U and K/U can be changed in an experiment by tuning the optical lattice laser intensities along each leg and by varying the separation between the legs, respectively. We assume up-down symmetry for the ladder, which implies that the chemical potential μ and the onsite interactions U are identical for each of the two legs. It is worth

noting that within the local density approximation, the results from this model can also be applied to experimental systems which have an additional harmonic trapping potential.

The phase α appearing in the hopping terms is given by $\alpha = (e/\hbar) \int_{r_j}^{r_k} d\mathbf{r} \cdot \mathbf{A}(\mathbf{r})$, where $\mathbf{A}(\mathbf{r})$ is the vector potential that gives rise to the magnetic field $\mathbf{B} = \nabla \times \mathbf{A}$ and r_j and r_k are the positions of the lattice sites j and k. If an atom tunnels around a plaquette, the total phase accumulated by the wave function is called the gauge flux, which is a gauge-invariant quantity. Specifically, we choose a Landau gauge for which the hopping in the rung direction has no gauge field while hopping along the legs imparts a phase that alternates from one plaquette to the next, leading to the required staggered flux. The physical properties of the Hamiltonian (1), including the energy spectrum, response functions, etc., are, of course, gauge invariant and only depend on the total flux going through a plaquette.

III. SINGLE-PARTICLE SPECTRUM

We first determine the structure of the single-particle energy spectrum as a function of the magnetic flux values. For this, we set $U = 0$ and write the Hamiltonian in momentum space in terms of the Fourier components of the field operators a_j and b_j. For ease of calculations, we use the gauge choice where the phase $e^{i\alpha}$ is only along one of the legs of the ladder, resulting in the same effective magnetic flux magnitude α for each plaquette. The energy eigenvalues can then be determined by simple diagonalization, and we show the spectrum as a function of momentum k in Fig. 2, for different absolute values of the magnetic flux α.

For zero flux and finite rung coupling, a two-band structure in the single-particle spectra appears, which has the expected 2π periodicity [see Fig. 2(a)]. In the presence of a finite staggered flux, the lowest band continues to have a nondegenerate minimum at $k = 0$ [see Figs. 2(b) and 2(c)] and increasing the
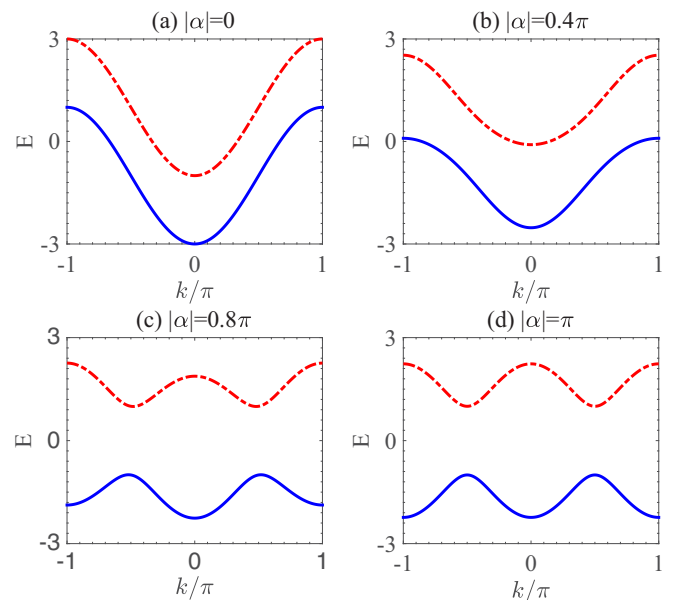

FIG. 2. Single-particle spectrum of the two-leg ladder system for different absolute magnetic flux strengths for $J = 1$ and $K = 1$.

rung coupling K leads to an increase in the band gap between the upper and lower bands. Since the system now possesses a finite flux, condensing into the minimum leads to a superfluid with a unique current pattern, which is further discussed in Sec. IV. Upon increasing the staggered flux further, the lowest band starts developing additional minima at $k = \pm\pi$ [see Fig. 2(c)], which eventually become degenerate with the minimum at $k = 0$ for $\alpha = \pi$ [see Fig. 2(d)]. This limit is known as the *fully frustrated* case for the Bose-Hubbard model and it corresponds to half a flux quantum per plaquette [25]. It is worth noting that at $\alpha = \pm\pi$ the presence of the two degenerate minima in the single-particle spectra is an indication of the nontrivial nature of superfluid phase with its unique current distribution, which we discuss below in Sec. VI B. The occurrence of degenerate minima at $k/\pi = 0$ and $k/\pi = \pm 1$ can influence the stability and properties of the phases in different regimes. While for the Mott-insulating regime the qualitative nature of the phase remains unaffected, the properties of the superfluid states can get substantially changed due to the staggered flux. We discuss this situation in detail in the next section.

IV. SUPERFLUID MOTT-INSULATOR TRANSITION: LANDAU THEORY OF PHASE TRANSITIONS

In this section, we discuss the results obtained for strong coupling regime and determine the complete phase diagram at zero temperature. For the Bose-Hubbard model with no flux, the zero-temperature phase diagram comprises a superfluid (SF) phase and a Mott insulator (MI) phase, which are separated by a second-order phase transition, driven by quantum fluctuations [31]. When one crosses the phase boundary from MI into the SF phase, the U(1) gauge symmetry is spontaneously broken, which gives rise to a finite SF-order parameter. Since the form of this order parameter depends on system parameters, one can expect that the presence of a finite staggered flux leads to different and distinctly broken-symmetry SF phases. In the following, we will use the Landau theory of phase transitions and introduce a plaquette order parameter, which identifies the various SF phases. Determining the values of U/J at which the SF order parameter vanishes allows us to obtain the phase boundaries within the full phase diagram as a function of the magnetic flux α.

The basic plaquette in our system consists of four sites, indicated by the dashed lines in Fig. 1. The different superfluid phases will be characterized by introducing the plaquette order parameter $\Psi = (\psi_1, \chi_1, \chi_2, \psi_2)$, where $\psi_i = \langle a_i \rangle$ and $\chi_i = \langle b_i \rangle$ stand for site order parameters for legs a and b, respectively. In the mean-field limit, we can decouple the sites of the unit cell by [32]

$$a_j^\dagger a_k \approx \psi_j^* a_k + a_j^\dagger \psi_k - \psi_j^* \psi_k,$$
$$b_j^\dagger b_k \approx \chi_j^* b_k + b_j^\dagger \chi_k - \chi_j^* \chi_k, \qquad (2)$$
$$a_j^\dagger b_j \approx \psi_j^* b_j + a_j^\dagger \chi_j - \psi_j^* \chi_j,$$

where $j, k \in \{1, 2\}$. Hence, we can write the mean-field Hamiltonian in the grand canonical ensemble in the form

$$H = H_0^{\mathrm{MF}} + H_1^{\mathrm{MF}},$$

where

$$H_0^{\mathrm{MF}} = \frac{U}{2} \sum_{j=1,2} \left[n_j^a \left(n_j^a - 1 \right) + n_j^b \left(n_j^b - 1 \right) \right] - \mu \sum_{j=1,2} \left(n_j^a + n_j^b \right) + K \sum_{j=1,2} (\psi_j^* \chi_j + \chi_j^* \psi_j) + J \left(e^{-\frac{i\alpha}{2}} \psi_1^* \psi_2 + e^{\frac{i\alpha}{2}} \chi_1^* \chi_2 + \mathrm{H.c.} \right)$$
$$+ J \left(e^{\frac{i\alpha}{2}} \psi_2^* \psi_3 + e^{-\frac{i\alpha}{2}} \chi_2^* \chi_3 + \mathrm{H.c.} \right), \qquad (3)$$

$$H_1^{\mathrm{MF}} = - J \left(e^{-\frac{i\alpha}{2}} \psi_1^* a_2 + e^{-i\frac{\alpha}{2}} \psi_2 a_1^\dagger + e^{i\frac{\alpha}{2}} \chi_1^* b_2 + e^{i\frac{\alpha}{2}} \chi_2 b_1^\dagger + \mathrm{H.c.} \right) - J \left(e^{\frac{i\alpha}{2}} \psi_2^* a_3 + e^{\frac{i\alpha}{2}} \psi_3 a_2^\dagger + e^{-\frac{i\alpha}{2}} \chi_2^* b_3 + e^{-\frac{i\alpha}{2}} \chi_3 b_2^\dagger + \mathrm{H.c.} \right)$$
$$- K \sum_{j=1,2} (\psi_j^* b_j + a_j^\dagger \chi_j + \mathrm{H.c.}). \qquad (4)$$

Since we concentrate on the strong-coupling regime, our expansion will treat H_1^{MF} as a perturbation. Calculating the ground-state energy, $E[\psi]$, for the four-site plaquette up to second order with respect to the perturbation H_1^{MF} then gives

$$E[\Psi] = 2Un(n-1) - 4\mu n + \sum_{\nu, \nu'} \Psi_\nu^* M_{\nu, \nu'} \Psi_{\nu'}, \qquad (5)$$

where n is the filling fraction and $M_{\nu, \nu'}$ are the matrix elements of the 4×4 Hermitian matrix M, which is given by

$$M = \begin{bmatrix} E_0(K^2 + 4J^2) & K & 4KJE_0\cos\left(\frac{\alpha}{2}\right) & 2Je^{-i\alpha/2} \\ K & E_0(K^2 + 4J^2) & 2Je^{i\alpha/2} & 4KJE_0\cos\left(\frac{\alpha}{2}\right) \\ 4KJE_0\cos\left(\frac{\alpha}{2}\right) & 2Je^{-i\alpha/2} & E_0(K^2 + 4J^2) & K \\ 2Je^{i\alpha/2} & 4KJE_0\cos\left(\frac{\alpha}{2}\right) & K & E_0(K^2 + 4J^2) \end{bmatrix},$$

with

$$E_0(n, U, \mu) = \left[\frac{n}{U(n-1) - \mu} + \frac{n+1}{\mu - Un} \right]. \qquad (6)$$

In standard Landau theory, the free energy is expanded with respect to a scalar order parameter and the phase-transition boundary is determined by demanding that the second-order expansion coefficient should vanish. In our case, the second-order phase transitions between the different SF and MI phases therefore occur when the eigenvalues of M are zero. The matrix has four eigenvalues and eigenvectors given by

$$\epsilon_1 = E_0[4J^2 + K^2 + 4JK\cos(\alpha/2)]$$
$$+ \sqrt{4J^2 + K^2 + 4JK\cos(\alpha/2)}, \qquad (7)$$

$$\epsilon_2 = E_0[4J^2 + K^2 - 4JK\cos(\alpha/2)]$$
$$+ \sqrt{4J^2 + K^2 - 4JK\cos(\alpha/2)}, \qquad (8)$$

$$\epsilon_3 = E_0[4J^2 + K^2 + 4JK\cos(\alpha/2)]$$
$$- \sqrt{4J^2 + K^2 + 4JK\cos(\alpha/2)}, \qquad (9)$$

$$\epsilon_4 = E_0[4J^2 + K^2 - 4JK\cos(\alpha/2)]$$
$$- \sqrt{4J^2 + K^2 - 4JK\cos(\alpha/2)}, \qquad (10)$$

$$\Psi_1 = \left(\frac{K + 2Je^{i\alpha/2}}{|K + 2Je^{i\alpha/2}|}, 1, \frac{K + 2Je^{i\alpha/2}}{|K + 2Je^{i\alpha/2}|}, 1 \right)$$
$$= (e^{i\theta_1}, 1, e^{i\theta_1}, 1), \qquad (11)$$

$$\Psi_2 = \left(-\frac{K - 2Je^{i\alpha/2}}{|K - 2Je^{i\alpha/2}|}, -1, \frac{K - 2Je^{i\alpha/2}}{|K - 2Je^{i\alpha/2}|}, 1 \right)$$
$$= (-e^{i\theta_2}, -1, e^{i\theta_2}, 1), \qquad (12)$$

$$\Psi_3 = \left(-\frac{K + 2Je^{i\alpha/2}}{|K + 2Je^{i\alpha/2}|}, 1, -\frac{K + 2Je^{i\alpha/2}}{|K + 2Je^{i\alpha}|}, 1 \right)$$
$$= (-e^{i\theta_1}, 1, -e^{i\theta_1}, 1), \qquad (13)$$

$$\Psi_4 = \left(\frac{K - 2Je^{i\alpha/2}}{|K - 2Je^{i\alpha/2}|}, -1, -\frac{K - 2Je^{i\alpha/2}}{|K - 2Je^{i\alpha}|}, 1 \right)$$
$$= (e^{i\theta_2}, -1, -e^{i\theta_2}, 1), \qquad (14)$$

where $\theta_1 = \tan^{-1}(\frac{2J\sin(\alpha/2)}{K + 2J\cos(\alpha/2)})$ and $\theta_2 = \tan^{-1}(-\frac{2J\sin(\alpha/2)}{K - 2J\cos(\alpha/2)})$. These four eigenvectors describe all possible SF phases.

A. Interpretation of the superfluid phases

In the standard Landau theory, the expansion of free energy is performed with respect to a scalar order parameter and the second-order phase transition point is determined by the vanishing of the second-order expansion coefficient. In the present work, we use an extension of this theory, where the second-order phase transitions is determined by the zero crossings of the eigenvalues of the matrix. Out of the four eigenvalues obtained in our calculations, the zero crossings of only the first two eigenvalues give physical phase boundaries between the superfluid and Mott-insulator phases for repulsive interactions in different regimes of magnetic flux. The other

two eigenvalues do not give any feasible boundaries for the case of repulsive interactions, indicating that they do not correspond to any physical superfluid phase.

In the following, we label the corresponding first two SF eigenvectors as superfluid 1 (SF-1) and superfluid 2 (SF-2), which, as they are not observables, have a form depending on the choice of the gauge in our calculations. They are, however, characterized by gauge-invariant circulating currents around the plaquettes, that are arranged in a staggered pattern along the ladder. In fact, these currents can be viewed as a sequence of vortices and antivortices, and we give more details about this below in Sec. VI B. The boson density is uniform for both superfluid states; however, the direction and sign of the leg and rung currents identify these states as having distinct patterns for currents related by time reversal or by a unit translation. Hence, SF-1 and SF-2 can be seen as corresponding to a single superfluid phase with two different order parameters depending on the strength of the magnetic flux. The condensate wave function appears due to the spontaneous breaking of the U(1) symmetry and a chiral current appears due to the symmetry broken explicitly by the Hamiltonian. This is consistent with the results known for the fully frustrated case with $\alpha = \pm\pi$ flux per plaquette, where Hartree theory indicates the presence of the same two superfluid states [25]. At this point, the Hamiltonian is invariant with respect to both translational and time-reversal symmetry, which leads to the emergence of the staggered flux states.

The phases of the order parameters at each lattice site are given by $\Phi_{\text{SF-1}} = (\theta_1, 0, \theta_1, 0)$ for SF-1 and $\Phi_{\text{SF-2}} = (\theta_2 + \pi, \pi, \theta_2, 0)$ for SF-2. In the fully frustrated case, which is the point where the system switches between being in SF-1 and SF-2, the phase around the plaquette for both superfluid states becomes equal and opposite, manifesting the opposite circulation of currents in each state. At this particular value of the magnetic flux, the energy eigenvalues of both superfluid states become degenerate as well, and while for $\alpha < \pi$ the SF-1 phase had the lower energy, beyond $\alpha = \pi$ the SF-2 become energetically more favorable. This transition from the SF-1 to the SF-2 phase therefore corresponds to a reversal of the direction of circulation.

B. Phase diagram

The boundary between the MI and SF phases can be found as a function of α by determining the zeros of the respective eigenvalues and we show the full phase diagram in Fig. 3. The zero crossings exist in the range $-\pi < \alpha < \pi$ for SF-1 and in the ranges $-3\pi < \alpha < -\pi$ and $\pi < \alpha < 3\pi$ for SF-2, implying a 2π periodicity for both the superfluid phases. As noted above, for values of α beyond $\pm\pi$, the SF-1 undergoes a transition to the SF-2, which at this point becomes energetically favorable ($\epsilon_2 < \epsilon_1$). The critical point of transition from SF to MI phase for $\alpha = 0$ agrees with the known mean-field results [18]. It is also worth nothing that at $\alpha = \pi$ and $-\pi$, for a gauge choice where the phase α is only along one of the legs, the Hamiltonian is real and therefore time-reversal invariant.

The phase diagram as a function of different values of the hopping amplitude K with fixed J is shown in Fig. 3. For $K < 1$, the hopping along the rung of the ladder is reduced,
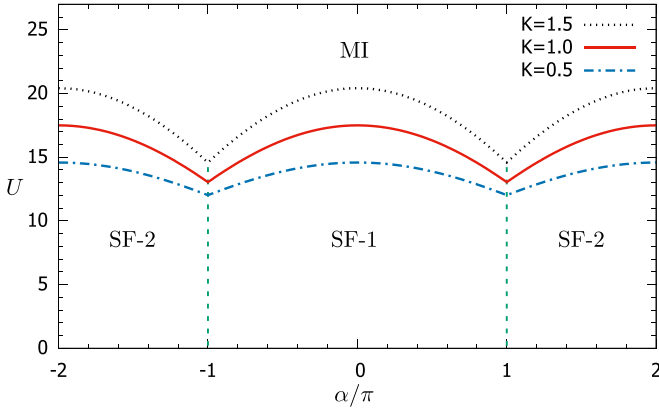
FIG. 3. Phase diagram for the two-leg ladder Bose-Hubbard model in the presence of a staggered flux of magnitude α for unit filling factor using Landau theory. The solid (red) curve marks the boundary between the Mott-insulator and the different superfluid phases for $K = J = 1.0$. The region below the solid (red) curve comprises of two types of superfluids, SF-1 and SF-2 (see text for details), which are separated by green dashed lines. The dashed (blue) lines and dotted (black) lines mark the phase boundaries for $J = 1$ and $K = 0.5$ and 1.5, respectively.

and hence the transition to the Mott-insulating state can be achieved at lower values of U. Similarly, for $K > 1$ the overall hopping is larger compared to the situation with $K = 1$ and the transition to the Mott-insulating phase requires a higher value of the onsite interaction U. This suggests that one can tune the phase transition boundary by simply changing the relative hopping amplitudes for any value of flux α.

V. VARIATIONAL MEAN-FIELD GUTZWILLER APPROACH FOR PHASE BOUNDARIES

In the following, we will explore the transition from the Mott insulator to the above-mentioned superfluid phases as a function of J, U, μ and α. For this, we scale the Hamiltonian in Eq. (1) by setting $K = 1$ and assume that the wave function for the perfect Mott-insulating phase is localized with an equal number of particles n_0 at each site. The phase boundary between the incompressible MI phase and the compressible SF phases can then be analytically determined by calculating the energy for particle-hole-type excitations using a reduced-basis variational ansatz for the Gutzwiller wave function.

For this, we assume that the total wave function is the product of two individual ladder wave functions, $|\Psi\rangle = \Pi_j |G\rangle_{a_j} |G\rangle_{b_j}$, where a and b label the legs of the ladder and j labels the individual sites along a leg. In the strongly interacting regime, we work very near to the phase boundary, which implies that only Fock states close to the MI one are populated. Hence, we can write a Gutzwiller ansatz for the local sites as

$$|G\rangle_{a_j} = f^{a_j}_{n_0-1}|n_0 - 1\rangle + f^{a_j}_{n_0}|n_0\rangle + f^{a_j}_{n_0+1}|n_0 + 1\rangle,$$

$$|G\rangle_{b_j} = f^{b_j}_{n_0-1}|n_0 - 1\rangle + f^{b_j}_{n_0}|n_0\rangle + f^{b_j}_{n_0+1}|n_0 + 1\rangle. \quad (15)$$
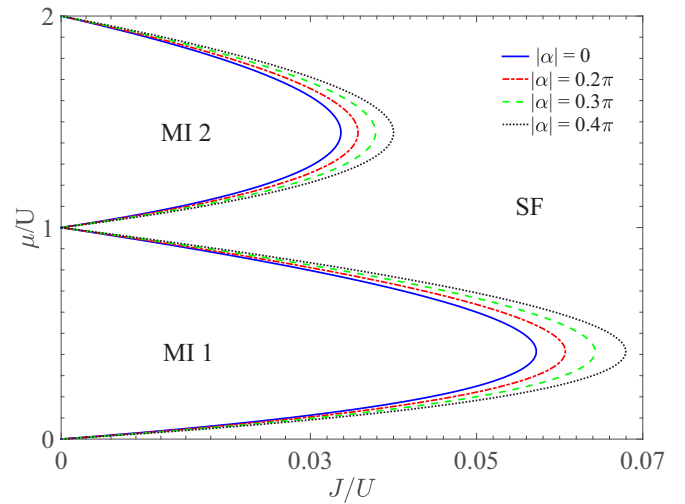

FIG. 4. Phase diagram of the Bose-Hubbard model for the two-leg ladder for different absolute values of staggered magnetic flux α, for $K = 1$ and $U = 1$, calculated using a variational mean-field approach. The MI phases are indicated with their average occupancy per site, and SF indicated in the plot can be SF-1 for $-\pi < \alpha < \pi$ and SF-2 for the regime $-3\pi < \alpha < -\pi$ and $\pi < \alpha < 3\pi$.

We parameterize the amplitudes as [33]

$$\left(f^{a_j}_{n_0-1}, f^{a_j}_{n_0}, f^{a_j}_{n_0+1}\right) = \left(e^{-i\theta_j}\Delta_{a_j}, \sqrt{1 - \Delta^2_{a_j} - \Delta'^2_{a_j}}, e^{i\theta_j}\Delta'_{a_j}\right),$$
$$(16)$$

$$\left(f^{b_j}_{n_0-1}, f^{b_j}_{n_0}, f^{b_j}_{n_0+1}\right) = \left(e^{-i\theta_j}\Delta_{b_j}, \sqrt{1 - \Delta^2_{b_j} - \Delta'^2_{b_j}}, e^{i\theta_j}\Delta'_{b_j}\right),$$
$$(17)$$

with complex variational parameters $\Delta_{a_j}, \Delta'_{a_j}, \Delta_{b_j}, \Delta'_{b_j} \ll 1$ to ensure the normalization condition of states $|G\rangle_{a_j}$ and $|G\rangle_{b_j}$. Minimizing the energy functional with respect to the variational parameters $\Delta_{a_j}, \Delta'_{a_j}, \Delta_{b_j}, \Delta'_{b_j}$, and θ_j gives the boundary between the MI and SF phase for any value of μ, U, and α. The dependence on the value of magnetic flux is implicit in the largest eigenvalue of the single-particle Hamiltonian and the Mott-insulator–superfluid phase boundaries are shown as a function of the magnetic flux α/π and interaction strength U in Fig. 4.

It can be seen that a higher magnetic flux enlarges the regions where the Mott-insulator phase appears by shifting the critical point or tip of the lobe for the phase transition to higher values. This enlargement of the insulating phase is expected since the effect of the magnetic field is to localize the single-particle dynamics even for noninteracting systems, thus making the transition to insulating phases easier. It is also known to occur for the case of bosonic two-leg ladder systems in the presence of uniform flux [18,20].

Let us stress that these results are exact within mean-field theory. The shape of the MI lobe is concave and independent of the dimensionality, since in our mean-field calculations the dimensionality enters only through a prefactor. Since fluctuations are known to be particularly important in lower dimensions, one cannot expect the mean-field theory to be

quantitatively accurate for quasi-one-dimensional systems. Hence, the results from the above analysis carry only qualitative importance and provide a general idea of how the phase boundaries are affected by the presence of magnetic flux. In particular, they can be expected to work only for small hopping strengths when correlations are weak. To complete our study, we present in the following numerical calculations for the phase diagram and the chiral currents.

VI. NUMERICAL RESULTS

In the following, we analyze the model given in Eq. (1) numerically using a self-consistent cluster mean-field theory (CMFT) approach. For this, a cluster of sites is considered as a unit cell of the system which is then decoupled from all other clusters using the mean-field decoupling approximation. For any two adjacent sites (i, j) which belong to different clusters, we therefore write

$$a_i^\dagger a_j \approx \phi_i^* a_j + a_i^\dagger \phi_j - \phi_i^* \phi_j, \qquad (18)$$

where $\phi_i^* = \langle a_i^\dagger \rangle$ and $\phi_j = \langle a_j \rangle$ are the SF order parameters. The resulting cluster Hamiltonian is then diagonalized self-consistently with respect to the superfluid order parameter ϕ_i, while keeping all other parameters fixed. The ground state obtained in this way can be used to calculate the number of particles at each site as $\rho_i = \langle n_i \rangle$.

CMFT takes into account the nonlocal correlations which are otherwise overlooked in the single-site mean-field method and it is therefore more accurate. With proper implementation, results from CMFT can match fairly well with those obtained from other sophisticated methods like quantum Monte Carlo, etc., but with significantly less computational efforts. Owing to these features, CMFT methods have been used extensively to successfully study a variety of problems in the past [34–42]. In this work, we use a four-site cluster as indicated by dashed lines in Fig. 1, fix the value of J as 1, and scale all other parameters in units of J.

A. Phase diagrams

The phase diagram calculated using the CMFT method is shown in Fig. 5. To obtain it, we first fix the value $K = 1$ and choose a particular value of $\alpha(=n\pi)$. We then fix U and vary μ to determine the ϕ_i self-consistently, and a vanishing value of ϕ_i along with an integer value of ρ_i signifies the SF-MI transition. To obtain the critical point for the SF-MI transition, we increase the value of U systematically until ϕ_i vanishes and ρ_i becomes equal to 1, or in other words until the system enters the Mott-insulator phase with filling factor 1. We repeat this procedure for several values of α varying from -2π to 2π and the critical values of U obtained in each case are marked by a black circle in the phase diagram in Fig. 5. The continuous red line connecting the black circles then indicates the SF-MI phase boundary and by comparing these to Fig. 3, one can clearly see that it matches the behavior obtained using the Landau theory of phase transitions presented in Sec. IV. Numerically studying the cases for $J = 1$ and $K \neq 1$ gives the corresponding shifts in phase boundaries as well (not shown).
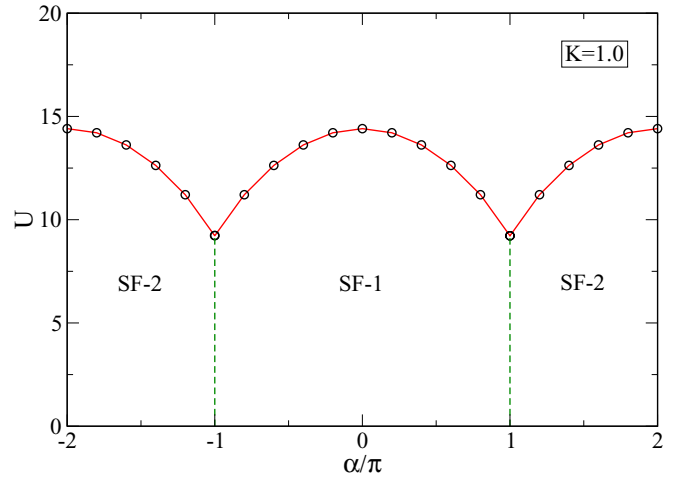

FIG. 5. Same as Fig. 3, but the results are obtained by using the CMFT approach.

B. Chiral currents

We finally calculate the chiral currents in the system using CMFT, which will allow us to determine the overall flow pattern in the system. The difference between the phases SF-1 and SF-2 can be characterized by their local current configurations and by their global chiral currents, the latter of which have the form

$$j_c = \sum_{l\in o/e} \langle j_{l,b}^{||} - j_{l,a}^{||} \rangle, \qquad (19)$$

where the associated operators are

$$j_{l,a}^{||} = i J (e^{-i\alpha/2} a_{l+1}^\dagger a_l - e^{i\alpha/2} a_l^\dagger a_{l+1}),$$
$$j_{l,b}^{||} = i J (e^{i\alpha/2} b_{l+1}^\dagger b_l - e^{-i\alpha/2} b_l^\dagger b_{l+1}). \qquad (20)$$

Here l represents the site index and for the numerical calculations we set the values of on-site interaction to $U = 8$ and of the chemical potential to $\mu = 11.5$, as for these parameters the system remains within the SF phase. The resulting chiral currents for different values of K are shown in Fig. 6. Two
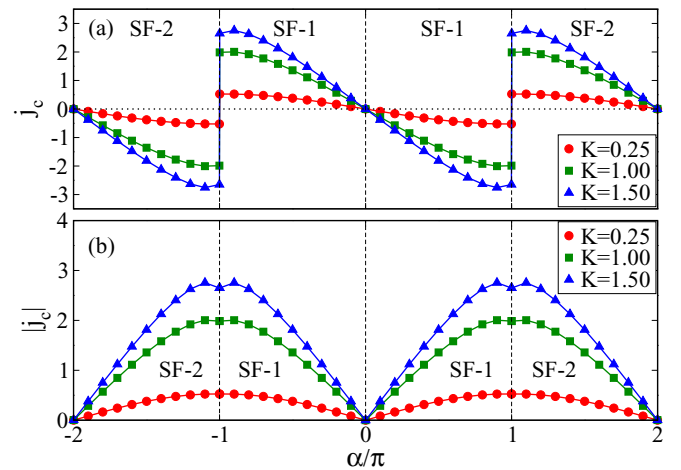

FIG. 6. Variation of j_c (top panel) and $|j_c|$ (bottom panel) with n for $J = 1$ and $K = 0.25, 1.0$, and 1.50 and $(U, \mu) = (8.0, 11.5)$.
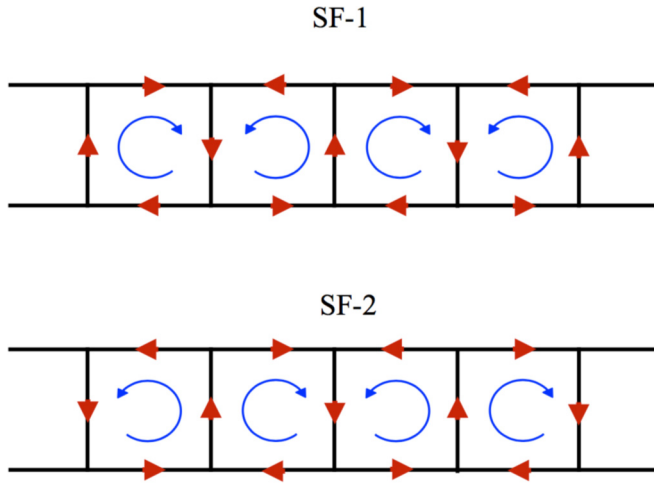
SF-1

SF-2

FIG. 7. Schematic of current patterns associated with the SF-1 and SF-2 phases. The red arrows denote the local currents given by equation (20). The blue circular arrows denote the local staggered vortices/antivortices deduced from the local current pattern. The local currents possess opposite rotational directions for the two superfluid phases.

striking features are immediately obvious: (i) The sign of j_c is reversed whenever the system makes a transition from the SF-1 to the SF-2 phase, while the sign of α is unchanged, and (ii) the slope of $|j_c|$ changes sign at the boundary between the two SF phases. The chiral currents for both SF-1 and SF-2 phases originate from the staggered currents going around each plaquette and have opposite rotational directions in each phase. For the SF-1 phase, the value of chiral currents increases as a function of increasing magnetic flux α, and local currents flowing around the plaquettes acquire a staggered (vortex-antivortex) configuration. At $\alpha = -\pi$ and π, the Hamiltonian becomes real and time-reversal invariant. Beyond these values, the staggered currents again break this symmetry, now with a reversal of the direction of the local currents around each plaquette, resulting in opposite chiral currents and a transition to SF-2 phase with a staggered (antivortex, vortex) current distribution. We want to highlight the fact that the only symmetry that is spontaneously broken here is the U(1) symmetry, which is responsible for giving the condensate phase and the origin of chiral currents is a result of the symmetry broken explicitly by the Hamiltonian. The flow of currents for both superfluid phases is schematically shown in Fig. 7. Although the value of μ is fixed to 11.5 for

the chiral current calculations, we have checked and found similar results for other values of μ as well, as long as the system is in the superfluid phase. The only change is in the absolute value of j_c.

It is to note that Fig. 6 shows the behavior of chiral currents as a function of magnetic flux for different values of rung tunneling K. It depicts that with increase or decrease in strength of rung tunneling, the chiral currents increase or decrease accordingly. This is done for a fixed value of interaction U, implying that the behavior of chiral current is directly proportional to the ratio of K/U. Hence, it is evident from Fig. 6 that for fixed K value the chiral currents decrease with increasing interaction strength.

VII. SUMMARY AND OUTLOOK

We have examined the Bose-Hubbard model in the presence of a staggered magnetic flux on a two-leg ladder configuration. We have shown that such a system possesses an interesting phase diagram, which is strongly influenced by the magnetic flux. The presence of alternating flux in the system leads to the appearance of a staggered current superfluid phase, which is different than the ones observed in the standard two-leg Bose Hubbard model with uniform flux. We have performed numerical cluster mean-field studies to confirm these analytically obtained phases. We believe that the model we have considered serves as an example for understanding the fundamental properties of lattices gases coupled to more complicated gauge fields, and can, in particular, stimulate experimental work on two-leg ladder bosonic systems in the presence of staggered gauge fields.

ACKNOWLEDGMENTS

[1] D. Jaksch, C. Bruder, J. I. Cirac, C. W. Gardiner, and P. Zoller, Phys. Rev. Lett. **81**, 3108 (1998).

[2] M. Greiner, O. Mandel, T. Esslinger, T. W. Hänsch, and I. Bloch, Nature (London) **415**, 39 (2002).

[3] M. Lewenstein, A. Sanpera, and V. Ahufinger, *Ultracold Atoms in Optical Lattices* (Oxford University Press, Oxford, UK, 2012).

[4] I. Bloch, J. Dalibard, and W. Zwerger, Rev. Mod. Phys. **80**, 885 (2008).

[5] M. Yasunaga and M. Tsubota, J. Low Temp. Phys. **148**, 363 (2007); R. A. Williams, S. Al-Assam, and C. J. Foot, Phys.

Rev. Lett. **104**, 050404 (2010); M. Aidelsburger, M. Atala, M. Lohse, J. T. Barreiro, B. Paredes, and I. Bloch, *ibid.* **111**, 185301 (2013); H. Miyake, G. A. Siviloglou, C. J. Kennedy, W. C. Burton, and W. Ketterle, *ibid.* **111**, 185302 (2013).

[6] Y.-J. Lin, R. L. Compton, A. R. Perry, W. D. Phillips, J. V. Porto, and I. B. Spielman, Phys. Rev. Lett. **102**, 130401 (2009); Y.-J. Lin, R. L. Compton, K. Jimenez-García, J. V. Porto, and I. B. Spielman, Nature (London) **462**, 628 (2009).

[7] M. R. Matthews, B. P. Anderson, P. C. Haljan, D. S. Hall, C. E. Wieman, and E. A. Cornell, Phys. Rev. Lett. **83**, 2498 (1999); K. W. Madison, F. Chevy, W. Wohlleben, and J. Dalibard, *ibid.*

84, 806 (2000); J. R. Abo-Shaeer, C. Raman, J. M. Vogels, and W. Ketterle, Science **292**, 476 (2001).

[8] M. Aidelsburger, M. Atala, S. Nascimbène, S. Trotzky, Y.-A. Chen, and I. Bloch, Phys. Rev. Lett. **107**, 255301 (2011).

[9] J. Struck, C. Ölschläger, M. Weinberg, P. Hauke, J. Simonet, A. Eckardt, M. Lewenstein, K. Sengstock, and P. Windpassinger, Phys. Rev. Lett. **108**, 225304 (2012).

[10] M. Aidelsburger, M. Lohse, C. Schweizer, M. Atala, J. T. Barreiro, S. Nascimbène, N. R. Cooper, I. Bloch, and N. Goldman, Nat. Phys. **11**, 162 (2015).

[11] M. Lohse, C. Schweizer, H. M. Price, O. Zilberberg, and I. Bloch, Nature (London) **553**, 55 (2018).

[12] M. Ö. Oktel, M. Niţă, and B. Tanatar, Phys. Rev. B **75**, 045133 (2007); R. O. Umucalilar and M. O. Oktel, Phys. Rev. A **76**, 055601 (2007); D. S. Goldbaum, and E. J. Mueller, *ibid.* **77**, 033629 (2008); R. Sachdeva, S. Johri, and S. Ghosh, *ibid.* **82**, 063617 (2010); R. Sachdeva and S. Ghosh, *ibid.* **85**, 013642 (2012); S. Powell, R. Barnett, R. Sensarma, and S. Das Sarma, *ibid.* **83**, 013612 (2011).

[13] D. R. Hofstadter, Phys. Rev. B **14**, 2239 (1976).

[14] A. Tokuno and A. Georges, New J. Phys. **16**, 073005 (2014).

[15] S. Uchino and A. Tokuno, Phys. Rev. A **92**, 013625 (2015).

[16] S. S. Natu, Phys. Rev. A **92**, 053623 (2015).

[17] E. Orignac and T. Giamarchi, Phys. Rev. B **64**, 144515 (2001).

[18] A. Keles and M. O. Oktel, Phys. Rev. A **91**, 013629 (2015).

[19] R. Wei and E. J. Mueller, Phys. Rev. A **89**, 063617 (2014).

[20] R. Sachdeva, M. Singh, and T. Busch, Phys. Rev. A **95**, 063601 (2017).

[21] M. Atala, M. Aidelsburger, M. Lohse, J. T. Barreiro, B. Paredes, and I. Bloch, Nat. Phys. **10**, 588 (2014).

[22] B. K. Stuhl, H.-I. Lu, L. M. Aycock, D. Genkina, and I. B. Spielman, Science **349**, 1514 (2015).

[23] M. Mancini, G. Pagano, G. Cappellini, L. Livi, M. Rider, J. Catani, C. Sias, P. Zoller, M. Inguscio, M. Dalmonte, and L. Fallani, Science **349**, 1510 (2015).

[24] T. Haug, L. Amico, R. Dumke, and L.-C. Kwek, Quantum Sci. Technol. **3**, 035006 (2018); L. Amico, D. Aghamalyan, F.

Auksztol, H. Crepaz, R. Dumke, and L.-C. Kwek, Sci. Rep. **4**, 4298 (2014).

[25] A. Dhar, M. Maji, T. Mishra, R. V. Pai, S. Mukerjee, and A. Paramekanti, Phys. Rev. A **85**, 041602(R) (2012); A. Dhar, T. Mishra, M. Maji, R. V. Pai, S. Mukerjee, and A. Paramekanti, Phys. Rev. B **87**, 174501 (2013).

[26] J. C. Budich, A. Elben, M. Lacki, A. Sterdyniak, M. A. Baranov, and P. Zoller, Phys. Rev. A **95**, 043632 (2017).

[27] L.-K. Lim, C. M. Smith, and A. Hemmerich, Phys. Rev. Lett. **100**, 130402 (2008).

[28] L.-K. Lim, A. Hemmerich, and C. M. Smith, Phys. Rev. A **81**, 023404 (2010).

[29] O. Tieleman, A. Lazarides, and C. Morais Smith, Phys. Rev. A **83**, 013627 (2011).

[30] J. Yao and S. Zhang, Phys. Rev. A **90**, 023608 (2014).

[31] M. P. A. Fisher, P. B. Weichman, G. Grinstein, and D. S. Fisher, Phys. Rev. B **40**, 546 (1989).

[32] K. Sheshadri, H. R. Krishnamurthy, R. Pandit, and T. V. Ramakrishnan, Europhys. Lett. **22**, 257 (1993).

[33] M. C. Gutzwiller, Phys. Rev. Lett. **10**, 159 (1963); Phys. Rev. **137**, A1726 (1965).

[34] P. Buonsante, V. Penna, and A. Vezzani, Laser Phys. **15**(2), 361 (2005).

[35] S. R. Hassan and L. de' Medici, Phys. Rev. B **81**, 035106 (2010).

[36] D. Yamamoto, A. Masaki, and I. Danshita, Phys. Rev. B **86**, 054516 (2012).

[37] T. McIntosh, P. Pisarski, R. J. Gooding, and E. Zaremba, Phys. Rev. A **86**, 013623 (2012).

[38] D.-S. Lühmann, Phys. Rev. A **87**, 043619 (2013).

[39] M. Singh, T. Mishra, R. V. Pai, and B. P. Das, Phys. Rev. A **90**, 013625 (2014).

[40] M. Singh, S. Mondal, B. K. Sahoo, and T. Mishra, Phys. Rev. A **96**, 053604 (2017).

[41] M. Singh, S. Greschner, and T. Mishra, Phys. Rev. A **98**, 023615 (2018).

[42] R. Bai, S. Bandyopadhyay, S. Pal, K. Suthar, and D. Angom, Phys. Rev. A **98**, 023606 (2018).